# Character of particle-hole excitations in $^{94}$Ru deduced from $\gamma$-ray angular correlation and linear polarization measurements

F. Ghazi Moradi,[1,*] C. Qi,[1] B. Cederwall,[1] A. Ataç,[1,†] T. Bäck,[1] R. Liotta,[1] M. Doncel,[1] A. Johnson,[1] G. de France,[2] E. Clément,[2] A. Dijon,[3] R. Wadsworth,[4] T. W. Henry,[4] A. J. Nichols,[4] H. Al-Azri,[4] J. Nyberg,[5] A. Gengelbach,[5] T. Hüyük,[6] B. M. Nyakó,[7] J. Timár,[7] D. Sohler,[7] Zs. Dombrádi,[7] I. Kuti,[7] K. Juhász,[8,‡] M. Palacz,[9] G. Jaworski,[10,9] S. M. Lenzi,[11] P. R. John,[11] D. R. Napoli,[12] A. Gottardo,[12] V. Modamio,[12] A. Di Nitto,[13,§] B. Yilmaz,[14] Ö. Aktas,[15,16] and E. Ideguchi[17]

[1]*Department of Physics, Royal Institute of Technology (KTH), SE-10691 Stockholm, Sweden*
[2]*Grand Accélérateur National d'Ions Lourds (GANIL), CEA/DSM - CNRS/IN2P3, F-14076 Caen Cedex 5, France*
[3]*CEA, DAM, DIF, F-91297 Arpajon, France*
[4]*Department of Physics, University of York, YO10 5DD York, United Kingdom*
[5]*Department of Physics and Astronomy, Uppsala University, SE-75121 Uppsala, Sweden*
[6]*Instituto de Física Corpuscular, CSIC-Universitat de València, E-46980 València, Spain*
[7]*MTA Atomki, H-4001 Debrecen, Hungary*
[8]*Department of Information Technology, University of Debrecen, H-4032 Debrecen, Hungary*
[9]*Heavy Ion Laboratory, University of Warsaw, 02-093, Warsaw, Poland*
[10]*Faculty of Physics, Warsaw University of Technology, 00-662, Warsaw, Poland*
[11]*Dipartimento di Fisica e Astronomia, Università di Padova, and Istituto Nazionale di Fisica Nucleare, Sezione di Padova, I-35131 Padua, Italy*
[12]*Istituto Nazionale di Fisica Nucleare, Laboratori Nazionali di Legnaro, I-35020 Legnaro, Italy*
[13]*Instituto Nazionale di Fisica Nucleare, Sezione di Napoli, I-80126 Napoli, Italy*
[14]*Department of Physics, Ankara University, 06100 Tandoğan, Ankara, Turkey*
[15]*Department of Physics, Middle East Technical University, 06531 Ankara, Turkey*
[16]*Department of Physics, Necmettin Erbakan University, 42090 Konya, Turkey*
[17]*Research Center for Nuclear Physics, Osaka University, Ibaraki, 567-0047 Osaka, Japan*

(Received 14 November 2013; published 3 January 2014)

Linear polarization and angular correlations of $\gamma$-rays depopulating excited states in the neutron-deficient nucleus $^{94}_{44}$Ru$_{50}$ have been measured, enabling firm spin-parity assignments for several excited states in this nucleus. The deduced multipolarities of strong transitions in the yrast structure were found to be mostly of stretched $M1$, $E1$, and $E2$ types and, in most cases, in agreement with previous tentative assignments. The deduced multipolarity of the 1869 keV and the connecting 257 and 1641 keV transitions indicates that the state at 6358 keV excitation energy has spin parity $12^-_1$ rather than $12^+_3$ as proposed in previous works. The presence of a $12^-_1$ state is interpreted within the framework of large-scale shell-model calculations as a pure proton-hole state dominated by the $\pi(p^{-1}_{1/2} \otimes g^{-5}_{9/2})$ and $\pi(p^{-1}_{3/2} \otimes g^{-5}_{9/2})$ configurations. A new positive-parity state is observed at 6103 keV and is tentatively assigned as $12^+_2$. The $14^-_1$ state proposed earlier is reassigned as $13^-_4$ and is interpreted as being dominated by neutron particle-hole core excitations. The strengths of several $E1$ transitions have been measured and are found to provide a signature of core-excited configurations.

DOI: 10.1103/PhysRevC.89.014301 PACS number(s): 25.70.Gh, 29.30.Kv, 24.70.+s, 21.60.Cs

## I. INTRODUCTION

The structural features of atomic nuclei near the presumed doubly magic nucleus $^{100}$Sn have attracted the attention of numerous theoretical and experimental studies in recent years (see, e.g., Ref. [1] and references therein). For example, the stability of the $N = Z = 50$ shell closures have been questioned in several studies (see, e.g., Refs. [2–4]). However, such conclusions are contradicted by more recent lifetime and Coulomb-excitation studies [5–7] as well as $\beta$-decay studies for nuclei in this region [8,9], which confirm the standard picture of large $N = Z = 50$ shell gaps of around 6 MeV. The main structural properties of low-lying states in nuclei just below the $N = Z = 50$ shell closures can be well described within the relatively isolated $0g_{9/2}$ and $1p_{1/2}$ subshells. Of particular interest is the neutron-proton pair coupling scheme in the $N = Z$ nuclei [10,11] and the seniority structure of the $N = 50$ isotones. For example, the nuclei $^{96}$Pd and $^{94}$Ru show similar low-lying level yrast structures, reflecting approximate conservation of seniority symmetry up to seniority $v = 4$ and spin $I = 12$. Moreover, the second $4^+$ and $6^+$ states in $^{96}$Pd and $^{94}$Ru are predicted to show the dynamical conservation of the seniority symmetry [12–15]. A more realistic description of these nuclei may be obtained through large-scale shell-model (LSSM) calculations by including the neighboring $1p_{3/2}$ and $0f_{5/2}$ orbitals [16]. The lowest-lying (yrast) positive-parity

*Corresponding author: farnazg@kth.se
†Present address: Department of Physics, Ankara University, 06100 Tandoğan, Ankara, Turkey.
‡Deceased.
§Present address: Johannes Gutenberg-Universität Mainz, 55099 Mainz, Germany.

 

states in $^{94}$Ru, up to $12_1^+$, correspond to the lowest shell-model configuration, i.e., $\pi(0g_{9/2}^{-6})$. However, the second $12^+$ state (which is not possible in the $N = 50$ isotone $^{96}$Pd) is built on the configuration $\pi(0g_{9/2}^{-4}1p_{1/2}^{-2})$. This difference is the reason why the $12_2^+$ state is calculated to be well separated from the $12_1^+$ state by about 1.5 MeV. For higher-lying levels above the $12_2^+$ state, contributions from the orbitals $1p_{3/2}$ and $0f_{5/2}$, as well as core excitations involving the $0g_{7/2}$ and $1d_{5/2}$ proton and neutron orbitals, may also be important. A detailed study of the core-excited states in the $N = 50$ isotones $^{93}$Tc, $^{94}$Ru, and $^{95}$Rh was presented by Roth *et al.* [17], where mainly neutron core excitations $\nu(1d_{5/2}0g_{9/2}^{-1})$ were considered to play an important role.

A critical test of the accuracy of the shell-model wave functions may be provided by measurements of $E1$ transition strengths. Such strongly hindered $E1$ transitions related to core excitations were proposed for $^{96}$Pd and $^{97}$Ag [18,19]. $E1$ transitions are strictly forbidden considering only the model space spanning the orbitals $0g_{9/2}$, $1p_{1/2}$, $0g_{7/2}$, and $1d_{5/2}$. This is because the $E1$ transition operator only connects orbitals that differ by orbital angular momentum $\Delta l = 1$ and total angular momentum $\Delta j \leqslant 1$. Thus the observation of $E1$ transitions in nuclei in this region reveals information on the interplay between the deep-lying orbitals $0f_{5/2}$ and $1p_{3/2}$ and the high-lying orbitals $0g_{7/2}$ and $1d_{5/2}$ above the $N = Z = 50$ shell gap.

We here present new polarization and angular correlation measurements of $\gamma$-rays in $^{94}$Ru which enable us to deduce parities and angular momenta of excited states up to spin $20\hbar$. The previously reported level scheme was revised and compared with LSSM calculations. The strengths of forbidden $E1$ transitions were extracted from the measured lifetimes and are used to constrain the LSSM calculations.

## II. EXPERIMENTAL SETUP

The experiment was performed at the Grand Accélérateur National d'Ions Lourds (GANIL) in France. High-spin states in $^{94}$Ru were populated following the heavy-ion fusion-evaporation reaction $^{58}$Ni($^{40}$Ca,$4p$)$^{94}$Ru. The $^{40}$Ca ions, delivered by the CSS1 cyclotron of GANIL were accelerated to a kinetic energy of 125 MeV and impinged on an isotopically enriched (99.83%) $^{58}$Ni target of 6 mg/cm$^2$ thickness. Prompt $\gamma$-rays emitted from the reaction were recorded by the EXOGAM $\gamma$-ray spectrometer array [20], consisting of 11 Compton-suppressed HPGe segmented clover detectors placed in two rings at 90° and 135° relative to the direction of the beam. Coincident emission of charged particles and neutrons was recorded, respectively, by the charged-particle detector array DIAMANT [21,22], consisting of 80 CsI(Tl) scintillators and by the Neutron Wall [23], an array of 50 organic liquid-scintillator detectors covering a $1\pi$ solid angle in the forward direction. Proton and $\alpha$-particle detection efficiencies of DIAMANT were measured to be 65% and 55%, respectively. The hardware trigger condition for recording events for subsequent offline analysis was one detected $\gamma$-ray in any of the Ge clover detectors and at least one neutron-like event in the Neutron Wall. The latter signal was determined by a hardware threshold on the zero-crossing time of the signals from the Neutron Wall shaping amplifiers. This hardware condition was sufficiently relaxed to allow also a fraction of the events where no neutrons were detected to be recorded. The final discrimination between neutrons and $\gamma$-rays in the Neutron Wall was performed offline by setting two-dimensional gates on the neutron time-of-flight versus the zero-crossover. For the offline charged-particle selection, 80 individual two-dimensional gates on the "particle identification" and "energy" parameters of DIAMANT enabled the identification of $\gamma$-rays as belonging to specific charged-particle evaporation channels. A 50-ns-wide coincidence time gate was applied to the aligned Ge detector time spectra. The energy calibration was performed using standard radioactive sources ($^{60}$Co and $^{152}$Eu). The offline analysis of selected $\gamma$-ray matrices and spectra was performed using the RADWARE software package [24].

## III. POLARIZATION AND ANGULAR CORRELATION MEASUREMENTS

The most practical technique for detecting the linear polarization, known as direction-polarization correlation (DPC), is based on the fact that the angular distribution of Compton scattered $\gamma$-rays is sensitive to the polarization state of the photon. The principal information that can be obtained from such a measurement is the character of the polarized electromagnetic radiation emitted from excited nuclear states. In this technique, the angle of the linear polarization vector of incident $\gamma$-rays on a scatterer can be measured relative to the scattering plane containing the incident and Compton-scattered $\gamma$-ray momentum vectors. Hence, information about the polarization of the $\gamma$-rays can be extracted by measuring the relative intensities at different scattering angles. The application of composite $\gamma$-ray detectors such as Compton polarimeters has been investigated for large segmented Ge-detector arrays such as EUROGAM and EXOGAM [25–28]. The previous multipolarity assignments of $\gamma$-rays from $^{94}$Ru are mainly based on angular distribution measurements [17] and are generally not conclusive. For example, it is not possible to distinguish between stretched electric and magnetic transitions of the same multipolarity solely from angular correlations. By measuring the sign and the degree of linear polarization this ambiguity can be removed for many observed $\gamma$-rays in the cascades. The granularity of the EXOGAM detector array with eight clover detectors placed in a ring at 90° relative to the beam direction makes it a suitable tool for measuring linear polarization of $\gamma$-rays. In this configuration, if we define the emission plane as the plane spanned by the incident beam direction and the emitted $\gamma$-ray, the degree of polarization can be obtained by measuring the number of Compton-scattered $\gamma$-rays "parallel" ($I_{0^\circ}$) and "perpendicular" ($I_{90^\circ}$) to this plane. For $^{94}$Ru such $\gamma$-ray events were analyzed by using $\gamma$-ray coincidence matrices gated on parallel-perpendicular scattering between the Ge crystals in clover detectors located in the ring at 90° relative to the beam axis. The gates were set on the $\gamma$-rays belonging to the $4p$ reaction channel detected in any clover. The intensities of the scattered $\gamma$-rays were used to calculate an experimental asymmetry parameter $A$, which is

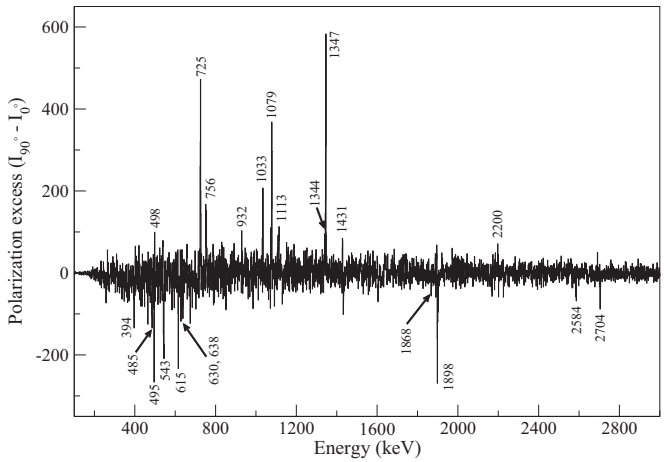


FIG. 1. $\gamma$-ray-asymmetry spectrum for $^{94}$Ru. The spectrum is obtained by subtracting the energy spectra corresponding to perpendicular and parallel scattering (see text) and is shown for illustrative purposes. The asymmetry values were extracted from Eq. (1) after fitting photopeak intensities in the individual spectra.

proportional to the degree of the linear polarization normalized to the corrected total intensity. The asymmetry parameter is defined as

$$A = \frac{a(E_\gamma) I_{90^\circ} - I_{0^\circ}}{a(E_\gamma) I_{90^\circ} + I_{0^\circ}} \quad (1)$$

The scaling factor $a(E_\gamma)$, related to the geometrical asymmetry of the EXOGAM clover detectors, was prepared in the same way as in Ref. [26], although with smaller statistical uncertainties. The linear fitting parameters were improved to $a_0 = 0.953\,(6)$ and $a_1 = 3.06\,(0.7) \times 10^{-5}$. As a sample spectrum the excess of polarization $(I_{90^\circ} - I_{0^\circ})$ for $^{94}$Ru is shown in Fig. 1. For example, assuming that the admixture of higher-order multipolarities is negligible, the positive $\gamma$-ray peaks may correspond to stretched $E1$ or stretched $E2$ radiation and the negative $\gamma$-ray peaks may correspond to stretched $M1$ or nonstretched $E1$ radiation. These ambiguities can be removed by additionally considering the directional angular correlation of the $\gamma$-rays.

For a pair of coincident $\gamma$-rays depopulating oriented nuclear states, the corresponding directional correlation function (often denoted as DCO) depends on the geometrical configuration of the detector system. The spins of excited levels in $^{94}$Ru are assigned based on angular correlation measurements by extracting the experimental angular correlation intensities for all possible combinations of detector pairs located at angles $\theta_1$ and $\theta_2$ with respect to the beam. For the EXOGAM array with 3 detectors at $\theta_1 = 135^\circ$ and eight detectors at $\theta_2 = 90^\circ$ the experimental DCO ratio is defined as

$$R_{DCO} = \frac{I_{\gamma_1}^{\theta_1}(\text{gated by } \gamma_2 \text{ at } \theta_2)}{I_{\gamma_1}^{\theta_2}(\text{gated by } \gamma_2 \text{ at } \theta_1)}, \quad (2)$$

where $I_{\gamma_1}^{\theta_1}$ and $I_{\gamma_1}^{\theta_2}$ are obtained from the corresponding asymmetrical 135° versus 90° and 90° versus 135° $\gamma$-$\gamma$ coincidence matrix, respectively. A theoretical calculation of the directional correlations [29] shows that by selecting on a pure stretched $E2$ transition, $\gamma_1$, $R_{DCO} \approx 0.6$ if $\gamma_2$ is a stretched dipole transition and $R_{DCO} \approx 1.0$ if $\gamma_2$ is a stretched quadrupole transition. In the present study the $R_{DCO}$ values are obtained by gating on clean $E2$ transitions using the assignments of Ref. [17]. The relevant part of the $^{94}$Ru level scheme with new assigned states ($12_2^+$, $12_1^-$, $13_4^-$) is shown in Fig. 2. The deduced values of asymmetry and $R_{DCO}$ are given together with the assigned values of spin and multipolarity for some of the observed $\gamma$-rays in Table I.

The measured asymmetry versus $R_{DCO}$ values for $\gamma$-rays in $^{94}$Ru, shown in Fig. 3, indicate that most of the assigned spins and parities proposed by Roth *et al.* [17] are consistent with our measurements; however, with a few notable exceptions. As can be seen in Fig. 3 the polarization of the 1869 keV $\gamma$-ray, depopulating the 6358 keV state, is found to be negative. This together with the $R_{DCO}$ measurement clearly show that the multipolarity of this stretched dipole transition is $M1$ rather than $E1$ as previously assigned in Ref. [17]. We therefore gave special attention to the multipolarity of the populating 257 keV transition, which was not assigned in Ref. [17]. Since this transition is an energy doublet, different sets of gates were required to distinguish the polarization between these doublet transitions residing in the positive- and negative-parity bands [marked by (a) and (b), respectively, in Table I]. The result, which is shown in Fig. 3, indicates that the multipolarity of the 257 keV $\gamma$-ray feeding the level decaying by the 1869 keV transition is of stretched $E1$ type. The 257 keV $\gamma$-ray that connects the $17_1^-$ and $16_1^-$ states is of stretched $M1$ type, as suggested by Roth *et al.* [17]. The multipolarity of the 1641 keV $\gamma$-ray was also measured by setting gates on coincident transitions above and below this transition [marked as (d) in Table I]. Our results indicate that this transition is of nonstretched $E1$ type, as noted in Fig. 3. This transition is rather weak and both the $R_{DCO}$ and asymmetry values have large uncertainties. Therefore, additional information is needed to confirm this assignment. However, we may still conclude that the energy level at 6358 keV has spin parity $12^-$, and hence would be the first observed $12^-$ state in this nucleus.

A previous lifetime study of high-spin states in $^{94}$Ru measured the $11^-$(4489 keV) and $5^-$(2624 keV) levels to have lifetimes of 1097 and 731 ps, respectively [30]. As can be seen in Fig. 3 the deduced $R_{DCO}$ values for the 292 and 498 keV $\gamma$-rays depopulating the $11^-$ state are shifted towards lower and higher values, respectively and the $R_{DCO}$ value of 438 keV $\gamma$-ray depopulating the $5^-$ state is shifted towards higher values. This is likely due to the long lifetimes of the $11^-$ and $5^-$ levels attenuating the angular distribution of $\gamma$-rays depopulating these levels. A similar attenuation effect was also observed in the magnetic-moment measurement of the $11^-$ state by Jungclaus *et al.* [31]. We have also found reason to reassign the spin of the 7970 keV level energy that was previously assigned as $14_1^-$. The present polarization measurement reveals that the 532 keV transition feeding this level is of a pure stretched $E2$ character and since the spin parity of the 8501 keV level is found to be $15_2^-$, the spin of the 7970 level (previously assigned as $14_1^-$ in Ref. [17]) is reassigned as $13_4^-$. The multipolarity of the 733 keV transition depopulating the confirmed $15_2^-$ state is found to be of pure

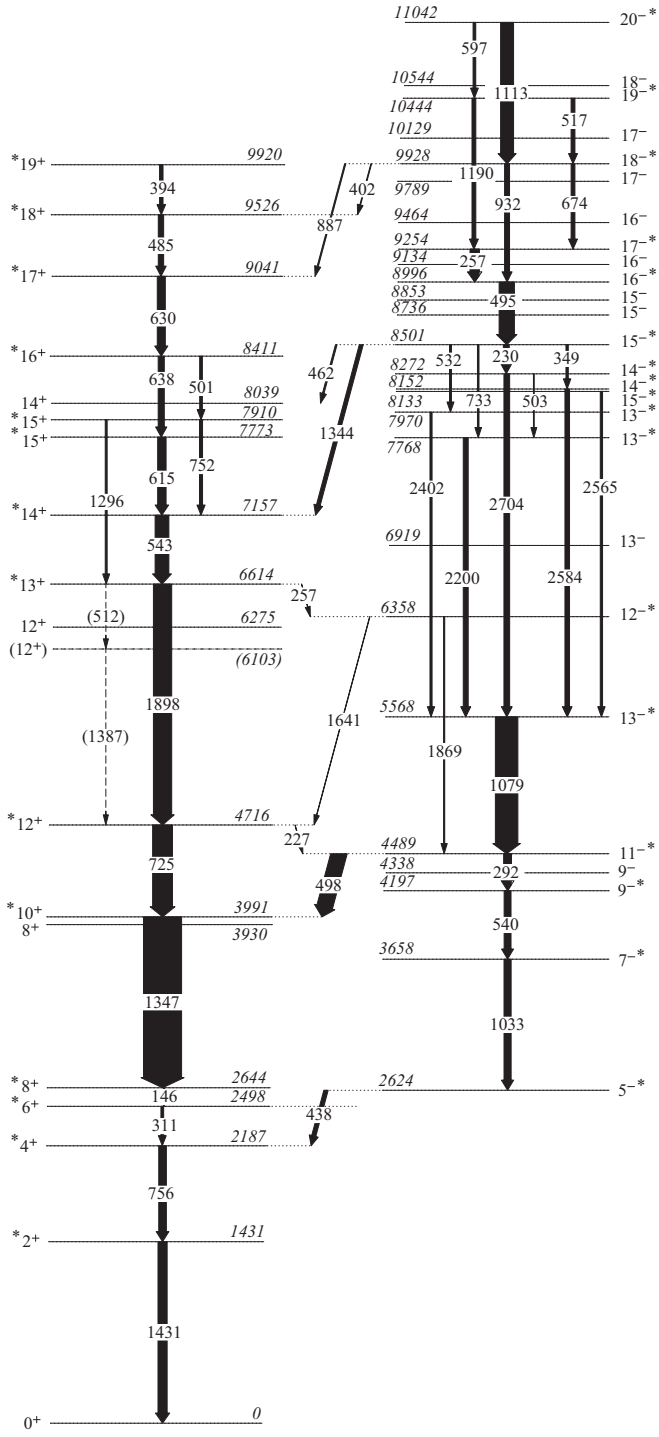


FIG. 2. Partial level scheme of $^{94}$Ru showing spins and parities deduced in the present work and in Ref. [17]. The stars indicate spins and parities confirmed by our asymmetry-$R_{DCO}$ measurement. The relative intensities were taken from Ref. [17].

TABLE I. $\gamma$-ray transition energies, asymmetry values A, $R_{DCO}$ ratios and spin-parity assignments for $^{94}$Ru. The transitions of reassigned multipolarities are marked by #. Only $\gamma$-rays for which both the asymmetry parameter and the angular correlation ratio could be deduced are listed here. Asymmetry values marked by letters indicate that sums of the coincidence gates: (a) 630, 638, and 394 keV, (b) 230, 733, and 1898 keV, (c) 2402, 495, 1079, 932, and 257 keV, (d) 725, 1347, 540, 498, and 257 keV, (e) 292, 540, 1033, and 1347 keV were used. The energy levels that have different spin-parity assignments than those previously assigned in Ref. [17] are marked by black dots. Statistical uncertainties are given in parentheses. $\Delta E_\gamma = \pm 0.5$ keV.

| $E_\gamma$ (keV) | $A$ | $R_{DCO}$ | $J_i^\pi \rightarrow J_f^\pi$ |
|---|---|---|---|
| 257.0# | 0.11 (17)[a] | 0.57 (9) | $13^+ \rightarrow 12^-_1$ • |
| 257.5 | −0.16 (18)[b] | 0.59 (6) | $17^-_1 \rightarrow 16^-_1$ |
| 292.3 | 0.16 (3) | 0.84 (5) | $11^- \rightarrow 9^-_1$ |
| 311.5 | 0.08 (8) | 1.17 (11) | $6^+ \rightarrow 4^+$ |
| 349.5 | −0.20 (15) | 0.45 (11) | $15^-_2 \rightarrow 14^-_1$ • |
| 394.5 | −0.08 (2) | 0.58 (8) | $19^+_1 \rightarrow 18^+$ |
| 438.3 | 0.04 (3) | 0.79 (4) | $5^- \rightarrow 4^+$ |
| 485.1 | −0.10 (1) | 0.55 (5) | $18^+ \rightarrow 17^+$ |
| 495.2 | −0.10 (1) | 0.65 (9) | $16^-_1 \rightarrow 15^-_2$ |
| 498.5 | 0.05( 2) | 0.72 (3) | $11^- \rightarrow 10^+$ |
| 501.5 | −0.13 (1) | 0.59 (15) | $16^+ \rightarrow 15^+_2$ |
| 503.5 | −0.01 (9) | 0.83 (16) | •$14^-_2 \rightarrow 13^-_3$ |
| 516.2 | −0.19 (13) | 0.51 (16) | $19^- \rightarrow 18^-_1$ |
| 531.6# | 0.17 (9)[c] | 1.07 (27) | $15^-_2 \rightarrow 13^-_4$ • |
| 540.0 | 0.10 (1) | 1.08 (9) | $9^-_1 \rightarrow 7^-$ |
| 543.4 | −0.108 (5) | 0.58 (4) | $14^+_1 \rightarrow 13^+$ |
| 615.6 | −0.08 (2) | 0.52 (5) | $15^+_1 \rightarrow 14^+_1$ |
| 630.1 | −0.106 (7) | 0.59 (5) | $17^+ \rightarrow 16^+$ |
| 638.5 | −0.12 (1) | 0.52 (5) | $16^+ \rightarrow 15^+_1$ |
| 674.1 | −0.26 (5) | 0.77 (18) | $18^-_1 \rightarrow 17^-_1$ |
| 725.0 | 0.123 (5) | 0.96 (5) | $12^+_1 \rightarrow 10^+$ |
| 733.0 | 0.14 (11) | 1.07 (24) | $15^-_2 \rightarrow 13^-_3$ |
| 752.6 | 0.05 (7) | 0.49 (6) | $15^+_2 \rightarrow 14^+_1$ |
| 756.4 | 0.062 (5) | 0.98 (4) | $4^+ \rightarrow 2^+$ |
| 932.1 | 0.05 (2) | 1.02 (14) | $18^-_1 \rightarrow 16^-_1$ |
| 1033.1 | 0.061 (7) | 1.01 (11) | $7^- \rightarrow 5^-$ |
| 1079.2 | 0.095 (5) | 1.14 (14) | $13^-_1 \rightarrow 11^-$ |
| 1113.5 | 0.08 (1) | 1.14 (18) | $20^-_1 \rightarrow 18^-_1$ |
| 1296.2 | 0.11 (5) | 1.04 (18) | $15^+_2 \rightarrow 13^+$ |
| 1344.4 | 0.18 (2) | 0.57 (14) | $15^-_2 \rightarrow 14^+_1$ |
| 1347.5 | 0.092 (3) | 1.01 (5) | $10^+ \rightarrow 8^+_1$ |
| 1430.9 | 0.023(5) | 0.94 (4) | $2^+ \rightarrow 0^+$ |
| 1641.0# | −0.26 (20)[d] | 1.05 (35) | •$12^-_1 \rightarrow 12^+_1$ |
| 1868.9# | −0.10 (4)[e] | 0.61 (14) | •$12^-_1 \rightarrow 11^-$ |
| 1898.2 | −0.043 (3) | 0.64 (5) | $13^+ \rightarrow 12^+_1$ |
| 2200.5 | 0.14 (6) | 1.06 (21) | $13^-_3 \rightarrow 13^-_1$ |
| 2401.7 | 0.01 (1) | 0.58 (12) | •$13^-_4 \rightarrow 13^-_1$ |
| 2565.0 | 0.1 (1) | 0.94 (20) | $15^-_1 \rightarrow 13^-_1$ |
| 2584.2 | −0.05 (1) | 0.58 (9) | •$14^-_1 \rightarrow 13^-_1$ |
| 2703.8 | −0.05 (1) | 0.58 (8) | •$14^-_2 \rightarrow 13^-_1$ |

stretched $E2$ character, which supports the assignment of $13^-_3$ to the 7768 keV level. The multipolarity of the 2704 keV transition depopulating the 8272 keV level is assigned as a pure stretched $M1$ which supports the assignment of $14^-_2$ to the 8272 keV level energy. Hence, the multipolarity of the 503 keV transition deexciting from the 8272 keV level to the 7768 keV level is also a stretched $M1$. Our measurement shows that the 503 keV transition has a very small negative asymmetry value while $R_{DCO}$ is somewhat larger than expected for a pure

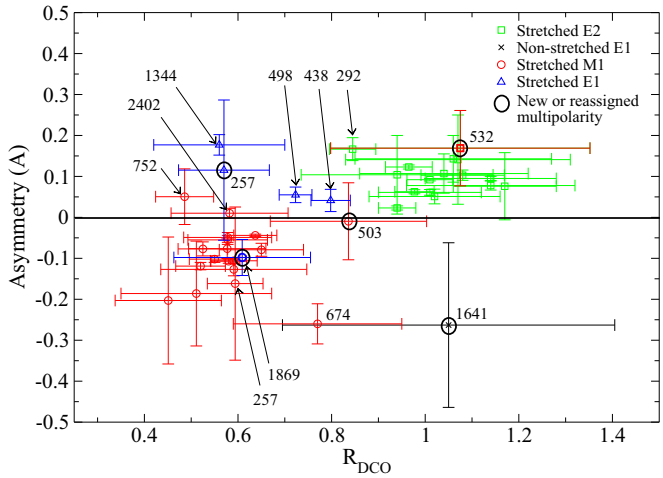


FIG. 3. (Color online) Deduced asymmetry parameter A vs $R_{DCO}$ values for $\gamma$-ray transitions in $^{94}$Ru. The stretched $M1$, stretched $E2$, stretched $E1$, and nonstretched $E1$ data points are shown as circles, squares, triangles, and stars, respectively. The color code indicates the assigned multipolarity by Roth *et al.* [17], where blue is stretched $E1$, red is stretched $M1$, and green is stretched $E2$. Some transitions of special interest are labeled by their energy values in keV (see text). Transitions of new or reassigned multipolarity are marked by black circles around the symbols.

stretched dipole transition (albeit with significant uncertainty). This "shift" of the asymmetry-$R_{DCO}$ values of the 503 keV transition from lower left to upper right in Fig. 3 might be an indication of a significant $E2$ multipole admixture. The deduced asymmetry of the 2402 keV transition is shifted towards more positive values. One explanation could be the presence of a doublet of different multipolarity (presumably $E1$) feeding from higher-spin states or an enhanced $E2$ admixture. The shift of the $R_{DCO}$ value of 674 keV $\gamma$-ray (stretched $M1$) towards higher values might also be due to $E2$ admixture.

In the positive-parity band two weak transitions in cascade, 512 and 1387 keV, were observed connecting the first $13^+$ state and the first $12^+$ state. Due to their low photopeak intensities it was not possible to measure polarization and angular correlations and to determine the ordering of these transitions unambiguously. However, we suggest an intermediate state at 6103 keV with a tentative spin-parity assignment of $12_2^+$. The multipolarity of the 1296 keV $\gamma$-ray was found to be of stretched $E2$ type, in agreement with the assignment of Ref. [17], confirming the spin parity of $15_2^+$ for the 7910 keV level. The 543 keV transition, which depopulates the $14_1^+$ state, is a pure stretched $M1$. Therefore, the multipolarity of the 752 keV transition depopulating the $15_2^+$ state is adopted as a stretched $M1$ even though a positive shift in the polarization value of the 752 keV transition is noted and might be due to contaminating transitions (the 756 keV in the positive-parity band and the low-lying 750 keV from $^{93}$Tc which have a strong $E2$ character).

The lifetimes of some high-spin states in $^{94}$Ru reported in Ref. [30] were used together with the measured relative intensities to extract partial decay rates and reduced transition probabilities of $E1$ transitions between the positive- and the negative-parity states. The results are shown in Table II.

TABLE II. The hindrance factors[a] $H$ for the observed $E1$ $\gamma$-ray transitions as deduced from the branching ratios and lifetimes [30] of the initial states. Uncertainties are given in parentheses. $\Delta E_\gamma = \pm 0.5$ keV.

| $E_\gamma$ (keV) | $J_i^\pi \rightarrow J_f^\pi$ | $H \times 10^5$ (W.u.)$^{-1}$ |
|---|---|---|
| 257 | $13^+ \rightarrow 12_1^-$ | 0.006 (1) |
| 462 | $15_2^- \rightarrow 14_2^+$ | 0.051 (5) |
| 402 | $18_1^- \rightarrow 18^+$ | 0.188 (25) |
| 1344 | $15_2^- \rightarrow 14_1^+$ | 0.451 (32) |
| 227 | $12_1^+ \rightarrow 11^-$ | 0.57 (27) |
| 887 | $18_1^- \rightarrow 17^+$ | 1.09 (12) |
| 438 | $5^- \rightarrow 4^+$ | 1.90 (17) |
| 498 | $11^- \rightarrow 10^+$ | 4.27 (19) |

[a] $H = \frac{A^{2/3}}{15.5 \times B(E1)}$.

## IV. DISCUSSION

Based on the observed $\gamma$-$\gamma$ coincidences and angular distribution measurements the level scheme of the semimagic ($N = 50$) $^{94}$Ru nucleus was previously interpreted as two main even- and odd-parity groups of states built primarily on proton single-particle structures from the $0g_{9/2}$ and $1p_{1/2}$ subshells [17,30,31]. The spin-parity assignments for some of the strongest populated states deduced in this work from linear polarization and angular correlation measurements confirm, unambiguously, this picture. The experimental energy levels with spin $I \leqslant 12$ (including the $12_1^+$ state) in the positive-parity structure and spin $I \leqslant 13$ (including the $13_1^-$ state) in the negative-parity structure are dominated by the $\pi(0g_{9/2}^{-6})$ and $\pi(1p_{1/2}^{-1}0g_{9/2}^{-5})$ configurations, respectively. The agreement between calculated and experimental level energies for these states is typically quite good while, for states above 6 MeV excitation energy, the precision of the theoretical predictions is significantly reduced. Several calculations using different shell-model configuration spaces have been performed [17,18,30,32,33] in order to interpret the structure of high-lying states above $I \geqslant 13$. The calculation presented in Ref. [32] was done in the model space $1p_{1/2}0g_{9/2}$, allowing also for an excitation of one neutron or proton to the $1d_{5/2}$ shell above the $N = Z = 50$ shell gap and it was found that neutron core excitations $\nu(1d_{5/2}^1 0g_{9/2}^{-1})$ play an important role. This is supported by the more recent calculations presented in Refs. [30,33].

Following the experimental findings presented in this work we have performed detailed shell-model calculations in order to further illuminate the structure of this semimagic nucleus. The calculations support our reassignment of the previous $12_3^+$ state [17] as $12_1^-$, and the previous $14_1^-$ state, which is interpreted as $13_4^-$ in the present work. In our LSSM calculations, where we take $^{100}_{50}$Sn$_{50}$ as the core, we first included the shells $1p_{1/2}, 1p_{3/2}, 0f_{5/2}, 0g_{9/2}$ (denoted as $fpg$ model space) with a maximum obtainable spin of $I = 16\hbar$. The effective interaction matrix elements from Ref. [16] were

adopted in this case. It is to be noted that the maximum spin states in Ref. [17] have values $I = 15\hbar$ since the model space is truncated by allowing at most one proton-hole excitation from the $0f_{5/2}$ and $1p_{3/2}$ orbitals. For comparison, and to understand the influence of high-lying configurations, we also evaluated the spectrum of $^{94}$Ru within the very small subspace containing only the shell $0g_{9/2}$ (denoted as $g$ model space) and also the somewhat larger subspace spanned by the subshells $1p_{1/2}0g_{9/2}$ (denoted as $pg$ model space). The interactions in these cases were taken from Refs. [11,34].

In Fig. 4 the experimental data are compared with the calculated level energies. One can see that the positive-parity states up to 3 MeV, as well as the states $10_1^+$ (at 3991 keV in the experimental spectrum) and $12_1^+$ (at 4716 keV) are well described by the $pg$ model space. Moreover, the positive-parity states are also well described by the $g$ space, i.e. in terms of the $0g_{9/2}$ shell only. One can consider the agreement between the experimental spectrum and the calculated spectra provided by the $g$-space as well as those from the $pg$-space a measure of the stiffness of the $N = Z = 50$ shell closure as well as of the semiclosed shell $Z = 38$.

In the present work, a new state is suggested at 6103 keV which is tentatively assigned as $12_2^+$ and is merely 172 keV lower in excitation energy than the next $12^+$ state. Our shell-model calculations do not reproduce two nearly degenerate $12_2^+$ and $12_3^+$ states in this region when a limited model space is used. As can be seen from Fig. 4 the $fpg$ calculation predicts the energy gap between the second and the third calculated $12^+$ state to be around 600 keV. This is because the third $12^+$ state involves excitations from the shells $0f_{5/2}$ and $1p_{3/2}$. This gap is significantly reduced when core excitations are allowed. However, it is noteworthy that no firm spin-parity assignment could be obtained for the tentative $12_3^+$ 6275 keV state in this work.

The negative-parity states up to $13_1^-$ are all built upon the configuration $\pi(1p_{1/2}^{-1}0g_{9/2}^{-5})$. The lowest observed state of this configuration is $5^-$. The other observed states up to $13_1^-$ are built by excitations induced by the shell $0g_{9/2}$. In other words, the $1p_{1/2}$ proton state acts only as a spectator in these excitations, as already pointed out in Ref. [30]. Therefore, the structure of these states should be quite similar to the corresponding positive-parity states emerging from excitations of five proton holes in the shell $0g_{9/2}$. These are yrast positive-parity states in the nucleus $^{95}$Rh. That is, the states up to spin $13_1^-$ correspond to a $1p_{1/2}^{-1}$ proton state coupled to the low-lying positive-parity states in $^{95}$Rh. However, this appealing comparison has a limited validity for higher spins. Already the observed state $12_1^-$ in Fig. 4 is seen to be overestimated by more than 1.3 MeV by calculations performed within the $pg$ model space. This is because the $12_1^-$ wave function within the $pg$ model space provides only 85% of the total occupation probability of that state. In fact about 10% of the contribution to that total probability comes from the configuration $\pi(1p_{3/2}^{-1}0g_{9/2}^{-5})$. Therefore, the calculation using the extended model space $fpg$, which includes the $1p_{3/2}$ shell, predicts rather well the $12_1^-$ experimental energy as seen in Fig. 4. As summarized in Table II, there are a number of weak $E1$ transitions connecting states at low excitation energies (below 5 MeV). All states in this region are well described within the shell-model space spanned by $f_{5/2}$, $p_{3/2}$, $p_{1/2}$ and $g_{9/2}$ subshells. However, in this space there is no room for $E1$ transitions as mentioned above since the matrix elements $\langle f|E1|i\rangle$ vanish for all possible combinations of initial states $i$ and final states $f$. This indicates that other (higher or deeper lying) single-particle states are active here. Even a minute admixture of such configurations in the wave function may greatly increase the probability of $E1$ decay since the $E1$ single-particle matrix element is very large in comparison with any other multipole mode. Hence, the observed $E1$ transition strengths may serve as a critical test of the shell-model wave function with respect to the limited model subspace from which it is constructed.

We estimate the minor components of the wave functions contributing to the $E1$ transitions by opening the subshells $1d_{5/2}$ and $0g_{7/2}$ above the $N = Z = 50$ shell gap, which are connected to the deep-lying orbitals $1p_{3/2}$ and $0f_{5/2}$ through the $E1$ operator. Our expanded model space, denoted as $fpgd$, includes all orbitals between the $N = Z = 28$ and $N = Z = 64$ subshells. The $fpg$ part of the Hamiltonian is taken to be the same as for the $fpg$ calculations shown in Fig. 4. The remaining two-body interaction matrix elements involving the $0g_{7/2}$ and $1d_{5/2}$ orbitals are derived from the renormalized realistic CD-Bonn nucleon-nucleon potential [35], as was done in Refs. [5,36]. The effect of core excitations on the low-lying states may have partially been taken into account through the renormalization of the two-body interaction which is optimized by fitting to experimental data in this region [16]. To minimize double counting, we restricted our calculation so that at most one particle can be excited from below the $N = 50$ shell to the shells above. As in Ref. [5], for the cross-shell matrix elements we only consider those where the orbit $0g_{9/2}$ is involved.

In our Hamiltonian we explicitly consider the excitation of particles from the $f_{5/2}p_{3/2}p_{1/2}$ subshells to the $g_{9/2}$ subshell as well as those from the $g_{9/2}$ to $g_{7/2}$ or $d_{5/2}$ subshells. An $E1$ transition may occur if both excitations are present in our calculated wave function. The single-particle energies of the $0g_{7/2}$ and $1d_{5/2}$ orbitals are determined by fitting to known core-excited states in this region. As can be seen from Fig. 4, the results given by the $fpgd$ calculation for low-lying states up to around 6 MeV are similar to those of the $pg$ and $fpg$ model spaces, indicating that the influence of core excitation on these states is rather limited. The model space we choose here is similar to the so-called $fpgndg$ model space in Ref. [18]. There up to five particle-hole excitations across the $Z = N = 50$ shell closure is included in the LSSM calculation within the model space $0g_{9/2}$,$0g_{7/2}$,$1d_{5/2}$,$1d_{3/2}$,$1s_{1/2}$. However, as can be seen from the discussion above, the removal of the $1p_{1/2}$ and other deeper-lying orbitals may be problematic due to their important contribution to the structure and the $E1$ decay properties of many states discussed here.

The full theoretical description of the $E1$ transitions is a formidable task due to the huge dimension of the model space involved as well as the fact that the crucial configurations involved are tiny components of the nuclear wave function, the description of which requires highly accurate understanding of the underlying nuclear interaction. We estimate the $E1$

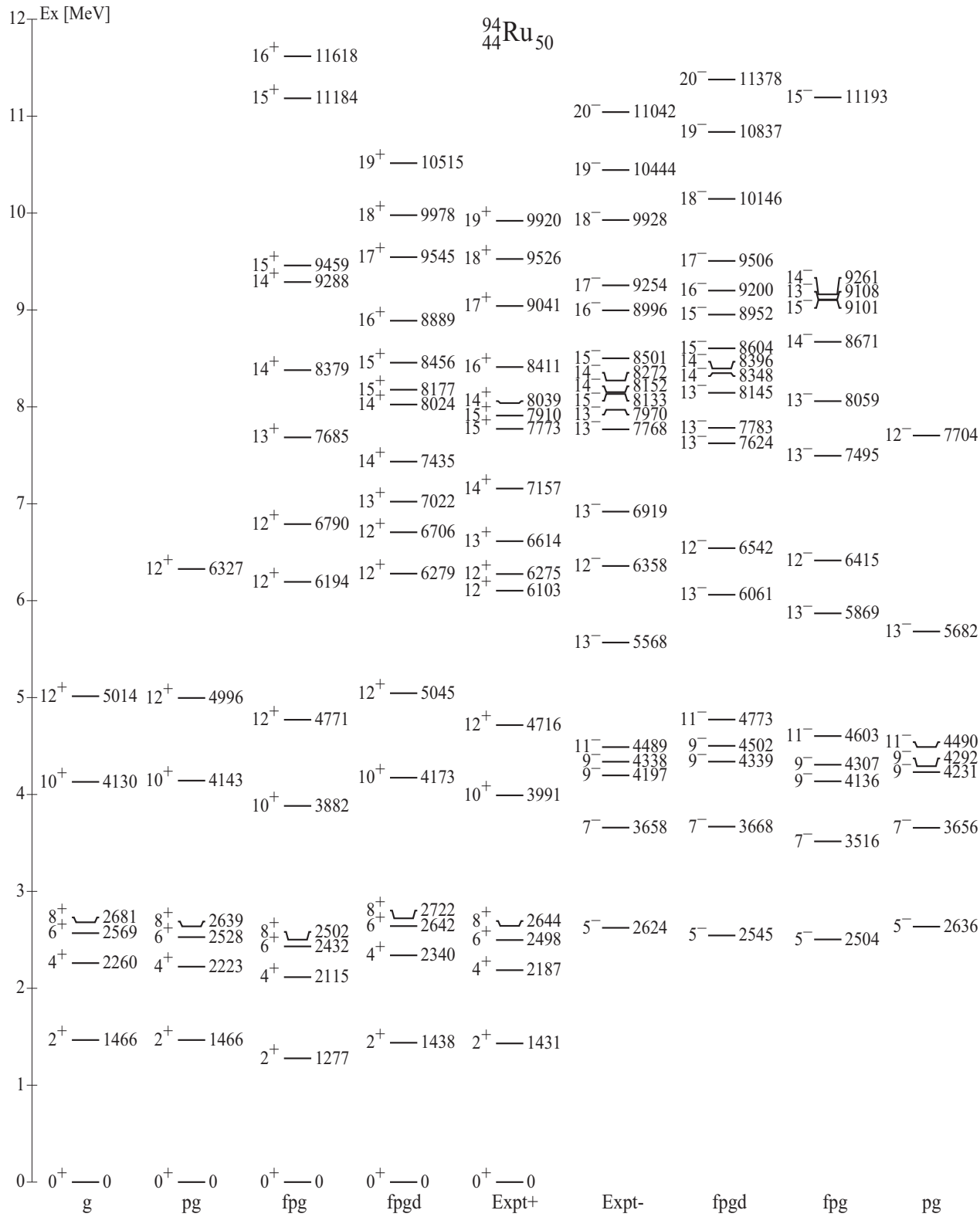


FIG. 4. Comparison between observed excitation energies and shell-model calculations for $^{94}$Ru. The experimental levels shown here are those for which the spins and parities were deduced in this work as well as some of the previously known levels from Ref. [17].

transitions between states accessible within this expanded shell-model space by evaluating the occupation probability of the different orbitals involved. As typical examples we consider the most hindered $E1$ transitions from the first $5^-$ state to the state $4^+$ as well as from the first $11^-$ state to the first $10^+$ state. The core-excitation components in these states are mainly of a one-neutron character. The contribution to the transition probability from the high-lying shells $1d_{5/2}$ and

$0g_{7/2}$ can be estimated from the occupation probability of these shells, which is around $10^{-2}$, while the contribution from the deep-lying shells $1p_{3/2}$ and $0f_{5/2}$ is $10^{-4}$. Therefore, the $E1$ transition probability which is proportional to the probability that the initial state is occupied while the final state is empty, will be of order $10^{-6}$ (W.u.). This is consistent with the experimental hindrance factors of 498 and 438 keV transitions given in Table II. The absence of $E1$ transitions depopulating the low-lying $13^-$ states indicates that the influence of the core-excited configurations is very limited for these states.

As mentioned above, the first $13^-$ state is dominated by the configuration $\pi(1p_{1/2}^{-1}0g_{9/2}^{-5})$. Calculations within the $fpg$ space show that the second $13^-$ state is determined mainly by the configuration $\pi(0f_{5/2}^{-1}0g_{9/2}^{-5})$. Both the third and the fourth $13^-$ states are dominated by the configuration $\nu(1d_{5/2}^{1}0g_{9/2}^{-1})\pi(1p_{1/2}^{-1}0g_{9/2}^{-5})$. That is, they are core-excited states being built from the first $13^-$ state with one neutron being excited from below the $N = 50$ shell closure to the $1d_{5/2}$ orbit. Our calculations show that the higher-spin states up to $20^-$ also contain one-neutron particle-hole excitations. This agrees with the calculations presented in Ref. [32]. The $12_3^+$ and $13_1^+$ states are predicted to be the lowest core-excited states on the positive-parity side. Both of them are dominated by the $\nu(1d_{5/2}^{1}0g_{9/2}^{-1})$ one-particle-hole excitation. This is the reason why the strongest $E1$ transition observed in the present work is found in the decay from the $13_1^+$ to the state assigned as $12_1^-$. The $12_1^-$ state contains a relatively large contribution from the $1p_{3/2}$ proton excitation. The $13^+ \rightarrow 12_1^-$ 257 keV transition is thus mutually enhanced by proton and neutron excitations. Moreover, for the same reason, the $M1$ transition, which carries $\Delta l = 0$, from the state $13_1^+$ to the state $12_1^+$ is very much hindered. It may be worthwhile to underline that if the particle-hole configurations inducing the $E1$ transitions would be dominant in the nuclear wave function, then the corresponding core excitations would include the giant dipole resonance (GDR). The main characteristic of the GDR is that all particle-hole configurations contribute with the same phase to the corresponding energy-weighted sum rule.

## V. SUMMARY

Excited states in $^{94}$Ru were populated via the $^{58}$Ni($^{40}$Ca,$4p$)$^{94}$Ru fusion evaporation reaction. $\gamma$-rays from different fusion evaporation reaction channels were detected and identified using the EXOGAM HPGe detector array coupledto the Neutron Wall liquid scintillator detector array and the DIAMANT charged-particle detector system. Directional correlation and polarization measurements of $\gamma$-rays from $^{94}$Ru confirmed the existence of the two positive- and negative-parity yrast structures in this nucleus and led to a slight revision of the previously known level scheme. The multipolarity of the 1869 keV $\gamma$-ray was found to be of $M1$ type and the connecting 257 keV of $E1$ type indicating that the state at the 6358 keV level energy has spin parity $12_1^-$ rather than $12_3^+$ as proposed in previous works. A new state in the positive-parity band was observed at 6103 keV and tentatively assigned as $12_2^+$. In the negative-parity structure the polarization and angular correlation measurement showed that the 532 keV transition is of a pure stretched $E2$ character rather than $M1$ and therefore the spin of the 7970 keV state was reassigned as $13_4^-$. The observed structures were compared to LSSM calculations. States up to $13\hbar$ were calculated, in close agreement with the observed levels. The observed high-spin states were studied by performing LSSM calculation using the $fpgd$ shell-model space allowing only one-particle excitations to the $1d_{5/2}$ or $0g_{7/2}$ subshells. The reduced transition probabilities for $E1$ transitions were deduced from the partial decay rates and branching ratios and the strengths of hindered $E1$ transitions were used to test the LSSM parameters. The results showed a fair agreement with the observed transition strengths. A reduced $E1$ hindrance factor was found to provide a signature of core-excited configurations.

## ACKNOWLEDGMENTS

This work was supported by the Swedish Research Council (VR) under Grants No. 621-2010-4723 and No. 621-2012-3805. The authors acknowledge the GAMMAPOOL Euroball owners committee for the use of the Neutron Wall and also the EXOGAM and DIAMANT Collaborations. We thank the operators of the GANIL cyclotrons for providing the beam, their cooperation, and technical support. We would also like to thank UK STFC for their collaboration. This work was supported in part by the Hungarian Scientific Research Fund, OTKA (Contract No. K100835) and French-Polish LEA COPIGAL and COPIN-IN2P3 agreements. The research leading to these results has received funding from the European Union's Seventh Framework Program under Grant Agreement No. 262010.

[1] T. Faestermann *et al.*, Prog. Part. Nucl. Phys. **85**, 69 (2013).
[2] A. Banu *et al.*, Phys. Rev. C **72**, 061305 (2005).
[3] C. Vaman *et al.*, Phys. Rev. Lett. **99**, 162501 (2007).
[4] A. Ekström *et al.*, Phys. Rev. Lett. **101**, 012502 (2008).
[5] T. Bäck *et al.*, Phys. Rev. C **87**, 031306 (2013).
[6] G. Guastalla *et al.*, Phys. Rev. Lett. **110**, 172501 (2013).
[7] T. Bäck *et al.*, Phys. Rev. C **84**, 041306 (2011).
[8] C. B. Hinke *et al.*, Nature (London) **486**, 341 (2012).
[9] B. S. Nara Singh *et al.*, Phys. Rev. Lett. **107**, 172502 (2011).
[10] B. Cederwall *et al.*, Nature (London) **469**, 68 (2011).
[11] C. Qi, J. Blomqvist, T. Bäck, B. Cederwall, A. Johnson, R. J. Liotta, and R. Wyss, Phys. Rev. C **84**, 021301(R) (2011).
[12] A. Escuderos and L. Zamick, Phys. Rev. C **73**, 044302 (2006).
[13] P. Van Isacker and S. Heinze, Phys. Rev. Lett. **100**, 052501 (2008).
[14] C. Qi, Phys. Rev. C **83**, 014307 (2011).
[15] C. Qi *et al.*, Nucl. Phys. A **884-885**, 21 (2012).
[16] M. Honma, T. Otsuka, T. Mizusaki, and M. Hjorth-Jensen, Phys. Rev. C **80**, 064323 (2009).
[17] H. A. Roth *et al.*, Phys. Rev. C **50**, 1330 (1994).

[18] M. Palacz *et al.*, Phys. Rev. C **86**, 014318 (2012).
[19] M. Palacz *et al.*, Acta Phys. Pol. B **44**, 491 (2013).
[20] J. Simpson *et al.*, Acta Phys. Hung. New Ser: Heavy Ion Phys. **11**, 59 (2000).
[21] J. N. Scheurer *et al.*, Nucl. Instrum. Methods Phys. Res., Sect. A **385**, 501 (1997).
[22] J. Gál *et al.*, Nucl. Instrum. Methods Phys. Res., Sect. A **516**, 502 (2004).
[23] O. Skeppstedt *et al.*, Nucl. Instrum. Methods Phys. Res., Sect. A **421**, 531 (1999).
[24] D. C. Radford, Nucl. Instrum. Methods Phys. Res., Sect. A **361**, 290 (1995).
[25] P. M. Jones *et al.*, Nucl. Instrum. Methods Phys. Res., Sect. A **362**, 556 (1995).
[26] Y. Zheng *et al.*, Phys. Rev. C **87**, 044328 (2013).
[27] K. Andgren *et al.*, Phys. Rev. C **76**, 014307 (2007).
[28] G. Duchêne *et al.*, Nucl. Instrum. Methods Phys. Res., Sect. A **432**, 90 (1999).
[29] K. S. Krane *et al.*, Nucl. Data Tables **11**, 351 (1973).
[30] A. Jungclaus *et al.*, Phys. Rev. C **60**, 014309 (1999).
[31] A. Jungclaus *et al.*, Eur. Phys. J. A **6**, 29 (1999).
[32] K. Muto *et al.*, Phys. Lett. **135B**, 349 (1984).
[33] I. P. Johnstone and L. D. Skouras, Phys. Rev. C **55**, 1227 (1997).
[34] L. P. Johnstone and L. D. Skouras, Eur. Phys. J. A **11**, 125 (2001).
[35] M. Hjorth-Jensen *et al.*, Phys. Rep. **261**, 125 (1995).
[36] C. Qi and Z. X. Xu, Phys. Rev. C **86**, 044323 (2012).